ACS APPLIED MATERIALS & INTERFACES

Research Article

Cite This: ACS Appl. Mater. Interfaces 2018, 10, 5373−5384

www.acsami.org

Adsorption and Diffusion of Lithium and Sodium on Defective Rhenium Disulfide: A First Principles Study

Sankha Mukherjee,[†] Avinav Banwait,[†] Sean Grixti,[†] Nikhil Koratkar,[‡,§] and Chandra Veer Singh*[,†,∥]

[†]Department of Materials Science and Engineering, University of Toronto, Toronto, Ontario M5S 3E4, Canada

[‡]Mechanical, Aerospace and Nuclear Engineering and [§]Materials Science and Engineering, Rensselaer Polytechnic Institute, Troy, New York 12180, United States

[∥]Department of Mechanical and Industrial Engineering, University of Toronto, 5 King's College Road, Toronto, Ontario M5S 3G8, Canada

Supporting Information

ABSTRACT: Single-layer rhenium disulfide (ReS_2) is a unique material with distinctive, anisotropic electronic, mechanical, and optical properties and has the potential to be used as an anode in alkali-metal-ion batteries. In this work, first principles calculations were performed to systematically evaluate the potential of monolayer pristine and defective ReS_2 as anodes in lithium (Li)- and sodium (Na)-ion batteries. Our calculations suggest that there are several potential adsorption sites for Li and Na on pristine ReS_2, owing to its low-symmetry structure. Additionally, the adsorption of Li and Na over pristine ReS_2 is very strong with adsorption energies of −2.28 and −1.71 eV, respectively. Interestingly, the presence of point defects causes significantly stronger binding of the alkali-metal atoms with adsorption energies in the range −2.98 to −3.17 eV for Li and −2.66 to −2.92 eV for Na. Re single vacancy was found to be the strongest binding defect for Li adsorption, whereas S single vacancy was found to be the strongest for Na. The diffusion of these two alkali atoms over pristine ReS_2 is anisotropic, with an energy barrier of 0.33 eV for Li and 0.16 eV for Na. The energy barriers associated with escaping a double vacancy and single vacancy for Li atoms are significantly large at 0.60 eV for the double-vacancy case and 0.51 eV for the single-vacancy case. Similarly, for Na, they are 0.59 and 0.47 eV, respectively, which indicates slower migration and sluggish charging/discharging. However, the diffusion energy barrier over a Re single vacancy is found to be merely 0.42 eV for a Li atom and 0.28 eV for Na. Overall, S single and double vacancies can reduce the diffusion rate by 10^3−10^5 times for Li and Na ions, respectively. These results suggest that monolayer ReS_2 with a Re single vacancy adsorbs Li and Na stronger than pristine ReS_2, with negligible negotiation with the charging/discharging rate of the battery, and therefore they can be used as an anode in Li- and Na-ion batteries.

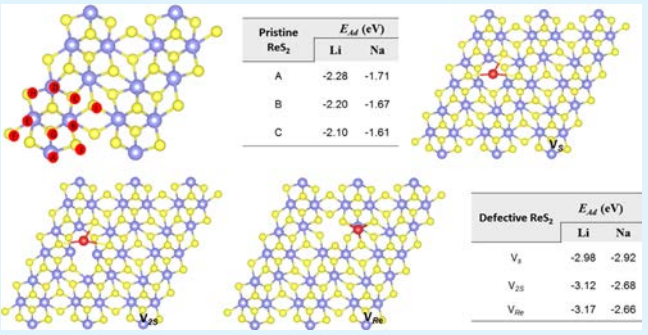

KEYWORDS: *Li/Na-ion battery, density functional theory, ReS_2, specific capacity, adsorption and diffusion*

1. INTRODUCTION

With the ever-increasing demand for light, and eco-friendly batteries with high power and energy densities,[1,2] low self-discharge rate, and comparatively long-term cycling stability[3] for running mobile devices and electrical vehicles (EVs), scientists are in constant search of suitable electrode materials. Alkali-metal (Li, Na)-ion batteries (AIBs) are potential candidates for the next-generation energy technology as they are portable, energy-efficient, and environmentally friendly.[4,5] The challenge associated with applying alkali-metal-ion batteries to EVs and portable appliances is obtaining a large storage capacity without compromising their long cycle lives and high charging/discharging rates.[6] The latter is determined by the ionic mobilities of alkali-metal ions in the electrode materials of the battery, which depend on the electronic interactions between the electrode and the alkali-metal ion. Thus, performance of these batteries is primarily dependent on the quality of the electrodes used. The performance of commercial lithium-ion batteries (LIBs), which use graphitic materials, oxides, and oxysalts as anode materials, is limited due to their poor power density arising from the low diffusivity of Li atoms within them. Practical solutions to some of these problems is to use anode materials with large surface areas and high Li atom diffusivities. In this regard, theoretical and experimental studies have reported that two-dimensional (2D) materials can be effectively used as anode materials in AIBs due to their large surface-to-volume ratios and exceptional electronic and mechanical properties. For example, alkali-

Received: September 7, 2017
Accepted: January 19, 2018
Published: January 19, 2018

DOI: 10.1021/acsami.7b13604
ACS Appl. Mater. Interfaces 2018, 10, 5373−5384

metal-ion batteries with anodes based of 2D materials, such as graphene,[7,8] phosphorene,[9−11] and borophene,[12,13] have been investigated because of their excellent electrochemical performance as battery electrodes. In particular, graphene anodes have been demonstrated to possess capacities in the range of 600 mAh/g compared to a theoretical capacity of 372 mAh/g for graphite-based LIBs.[7]

In the recent past, 2D transition-metal dichalcogenides (TMDs), which combine transition metals and chalcogenides, have attained increased attention from the electrode development community.[14−17] TMDs are layered structures, wherein different layers are held together by weak van der Waals forces. Unlike other 2D TMDs, ReS_2 has a direct band gap (1.47−1.61 eV)[18] and demonstrates a naturally distorted octahedral (1T) structure with a triclinic lattice, which provides unique chemical and electronic properties due to the lowered structural symmetry.[19] In bulk ReS_2, different atomic layers act electronically and vibrationally dissociated. As a result, the interlayer spacing in 2D ReS_2 is about 0.65−0.7 nm, compared to 0.33 nm for graphite, whereas the interlayer coupling energy is 18 meV compared to 460 meV in MoS_2.[20] Consequently, relatively large Li ions can migrate rapidly through ReS_2 without significant volumetric expansion, a problem critical to Si-based LIB anodes.[21] Recent experiments have demonstrated that LIBs made of ReS_2/graphene composites and few layers of ReS_2/carbon nanotube-based nanosheets possess capacities in the range of 300−900 mAh/g.[22,23] Additionally, we have recently demonstrated that vertically oriented arrays of ReS_2 nanosheets hold exceptional potential for use in Li−S batteries for energy storage.[24]

Ever since the discovery of monolayer ReS_2,[20] several top-down exfoliation-based techniques have been utilized for its synthesis, such as top-down mechanical exfoliation[25,26] and intercalation exfoliation[27] from its bulk counterparts. Additionally, chemical vapor deposition (CVD),[28,29] chemical vapor transport,[20,29] metal sulfurization,[30] and plasma-assisted method[31] have all been successfully utilized to fabricate 2D ReS_2. Generally, synthesis of 2D materials from bulk structures using deposition techniques or exfoliation comes at the cost of creating lattice defects in the final structure, such as point defects, and grain boundaries.[29] Thus, these structural defects alter the mechanical and electronic properties of the 2D structure significantly. For example, CVD-grown MoS_2 possesses inferior carrier mobility compared to their exfoliated counterparts. Also, point defects have been demonstrated to alter the magnetic properties of ReS_2[32] and $NbSe_2$[33] significantly. It has been reported that point defects in graphene[34] and MoS_2[35] increase the adsorption capability of Li ions and therefore increase the storage capacity of the battery. However, this increased adsorption strength can affect the diffusivity of the Li ions in the electrode due to increased chemical interaction between the substrate and the Li ions. For example, Sun et al.[35] reported that Li ions diffusion rates remain almost unaffected in MoS_2 with point defects and grain boundaries. In graphene, on the other hand, the rate of diffusion of Li atoms is more pronounced along a grain boundary compared to a direction perpendicular to the boundary.[36] Additionally, the rate of diffusion of Na over grain boundaries in graphene is more preferable over pristine graphene.[37] On the contrary, Zhang et al.[38] reported that single vacancies and double vacancies block the migration of Li ions over black phosphorous. These contradictions with different materials have lead us to raise the question of how lattice defects influence the adsorption and charging/discharging rates of Li and Na atoms in ReS_2-based batteries.

In this paper, the adsorption and diffusion of Li and Na atoms over ReS_2 via first principles density function theory (DFT) calculations have been reported. To the best of our knowledge, the adsorption and diffusion of Li and Na over defective ReS_2 have not been studied before. First, the favorable adsorption sites for the metal ions over pristine ReS_2 were identified, followed by the favorable adsorption sites for defective ReS_2 surfaces. Three distinct point defects, namely, sulfur single vacancy (SV), rhenium single vacancy, and sulfur double vacancy (DV), were created in the ReS_2 monolayers. These vacancies have been created in accordance with a previous DFT study on the stability and formation of point defects in ReS_2.[3939] Our calculations showed that binding energies for Li and Na atoms increase over defective ReS_2 compared to pristine monolayers. Additionally, charge density difference analysis and partial density of states calculations were performed to gain further insights into the adsorption process and characterize the electronic properties of Li- and Na-stuffed ReS_2 monolayers. Finally, climbing image nudged elastic band (CI-NEB) simulations were performed to determine the minimum-energy pathways (MEPs) and associated energy barriers for the Li and Na atoms adsorbed onto the surface of ReS_2.

2. COMPUTATIONAL METHODS

Plane-wave-based DFT simulations were conducted using the Perdew−Burke−Ernzerhof (PBE)[40] exchange-correlation functional within the generalized gradient approximation using the Quantum ESPRESSO package.[41] In addition, the Heyd−Scuseria−Ernzerhof (HSE06) functional was used to compute the band gap of pristine ReS_2. The atomic positions and lattice constants were optimized using the kinetic energy cutoff of 60 Ry for the wave functions and 480 Ry for the charge density, respectively. The convergence criterion of the self-consistent field procedure was set to 1×10^{-6} Ry. To avoid any interlayer interactions between ReS_2 surfaces from long-range van der Waals forces due to periodicity, a convergence test with respect to the box dimension in the z direction was performed (see Table S1), and a vacuum spacing of 15 Å was deemed sufficient. For binding energy computations, the position of every atom was relaxed using a conjugate gradient minimization over a $4 \times 4 \times 1$ Monkhorst−Pack[42] grid of k-points with the residual Hellmann−Feynman force on each atom less than 0.001 Ry/b. For structural analysis, all of the structures were visualized with XCrySDen[43] and VESTA.[44] The pristine ReS_2 supercell consisted of 2×2 unit cells (with 48 atoms), whereas the single-vacancy (SV) and double-vacancy (DV) supercells consisted of 3×3 unit cells (107 and 106 atoms, respectively). When calculating the adsorption energies of adsorbents over pristine and defective ReS_2, the dispersion corrections due to van der Waals forces were accounted by adopting the DFT + D approach.[45] To find the most stable adsorption positions, the alkali-metal atoms were placed above the sulfur atoms at different sites, followed by relaxation. The most stable adsorption site was determined by a comparison of the adsorption energies. The adsorption energy (E_{ad}) and charge density difference (ρ_{ad}) are determined by

$$E_{ad} = E_{adsorbed\ state} - (E_{adsorbent} + E_{substrate}) \quad (1)$$

$$\rho_{ad} = \rho_{adsorbed\ state} - (\rho_{adsorbent} - \rho_{substrate}) \quad (2)$$

where $E_{adsorbed\ state}$ represents the energy of monolayer ReS_2 after the adsorption of an alkali-metal atom, $E_{adsorbent}$ represents the energy of a single alkali-metal atom, and $E_{substrate}$ represents the energy of the monolayer ReS_2. A negative adsorption energy indicates that the adsorption is spontaneous and energetically favorable, with smaller values suggesting a stronger binding. Similarly, $E_{adsorbed\ state}$ is the

DOI: 10.1021/acsami.7b13604
ACS Appl. Mater. Interfaces 2018, 10, 5373−5384

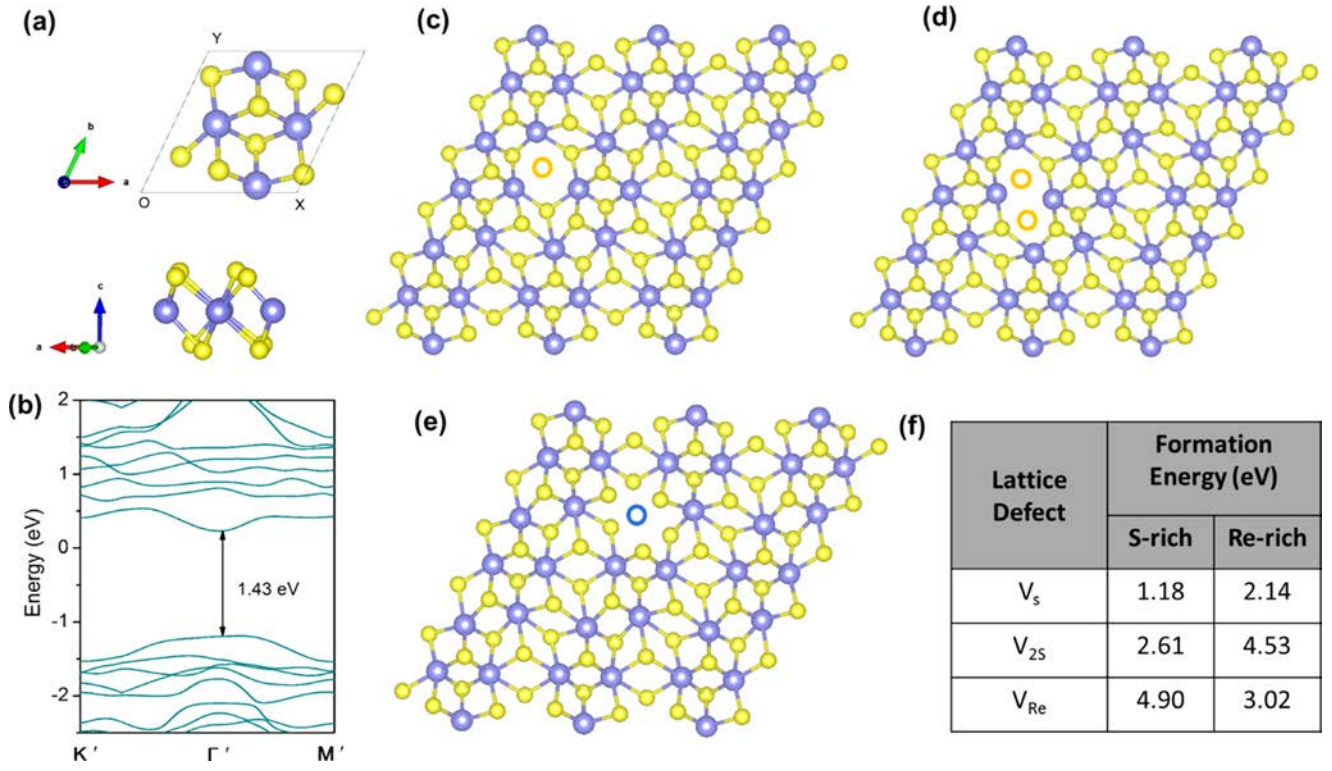

Figure 1. (a) Top view and side view of the unit cell of ReS_2. (b) Band structure of pristine ReS_2, with a band gap of 1.43 eV. Configurations of point defects in monolayer ReS_2. Top view of optimized structures of (c) V_S, (d) V_{2S}, and (e) V_{Re}. Hollow circles represent S (yellow) and Re (blue) atoms removed from the monolayer ReS_2. (f) Formation energies associated with the lattice defects under both S-rich and Re-rich conditions.

charge density of ReS_2 monolayer after alkali-metal adsorption, $\rho_{adsorbent}$ is the charge density of an alkali-metal atom, and $\rho_{substrate}$ represents the charge density of monolayer ReS_2. The average adsorption energy (E_{avg}) is calculated using the following equation

$$E_{avg} = \frac{E_{adsorbed\ state} - n \times E_{adsorbent} - E_{substrate}}{n} \quad (3)$$

where n represents the number of Li and Na atoms adsorbed, $E_{adsorbed\ state}$ represents the energy of the system after adsorption of all of the Li/Na atoms, $n \times E_{adsorbed\ state}$ represents the total energy of the Li or Na atoms, and $E_{substrate}$ represents the energy of pristine ReS_2. The open-circuit voltage (OCV) of the secondary battery is related to the total energy storage of the battery. As shown in previous works, this parameter may be estimated using the following relation under the assumption that volume and entropic terms are negligible[46−48]

$$OCV \approx \frac{-E_{avg}}{e} \quad (4)$$

where e is the elementary charge. The storage capacity of ReS_2 can be calculated using Faraday's equation, given by

$$q = 1000 \times F \times z\frac{n}{M_{ReS_2}} \quad (5)$$

where F, n, M_{ReS_2}, and z are Faraday's constant, the number of electrons involved in the electrochemical reaction, the mass of ReS_2, and the number of valence electrons involved in the electrochemical process, respectively. For studying the kinetics of diffusion of the adsorbent atoms over pristine and defective ReS_2 monolayers and calculating the associated energy barriers of diffusion, the climbing image nudged elastic band (CI-NEB) method[49] was utilized.

3. RESULTS AND DISCUSSION

3.1. Structure of Pristine and Defective ReS_2. Before discussing distinctive characteristics of alkali-metal adsorption over pristine and defective ReS_2, their relative stabilities and structural aspects are presented here. Unlike other TMDs, which have stable 1 hexagonal (H) (dichalcogens of Mo and W) and 1T (dichalcogens of Ti, V, and Ta) phases, ReS_2 has a distorted (1Td) phase, wherein four Re atoms group into Re_4 units to form ReS_2.[39] Tongay et al. calculated the phonon dispersion using the PBE functional and compared the results with experimental measurements of Raman spectra in ReS_2.[40] They showed that weaker interlayer interaction leads to decoupling of lattice vibrations between subsequent layers of ReS_2. Additionally, unlike other transition-metal dichalcogenides (TMDs), the LA and ZA phonon modes of periodic 1H and 1T structures of ReS_2 have imaginary frequencies and therefore are dynamically unstable. The distorted structure of 2D ReS_2 provides unique chemical and electronic properties. The distortion creates rhenium−sulfide bonds of varying lengths, with no single sulfur atom being in direct alignment with the ones surrounding it. In this study, the optimized parameters of the ReS_2 unit cell (Figure 1a) were found to be: OX = 6.54 Å, OY = 6.44 Å, and $\angle XOY$ = 61.15°.[9] The band diagram for pristine ReS_2 is shown in Figure 1b, which suggests a band gap of 1.43 eV. This band gap of ReS_2 is in excellent agreement with previous reports.[20] Because the PBE functional is known to underestimate band gap, HSE06 hybrid functional was used to obtain a more accurate electronic structure, which yielded a band gap of 2.41 eV for pristine ReS_2.

Due to its distorted structure, creating a defect at one site on the ReS_2 surface is not the same as creating a defect at another site. Thus, ReS_2 can have a vast variety of single and double vacancies of S and Re. Notably, whenever a vacancy defect is introduced on the ReS_2 surface, a substantial change in the overall structure occurs. The energetics and lattice structures of

DOI: 10.1021/acsami.7b13604
ACS Appl. Mater. Interfaces 2018, 10, 5373−5384

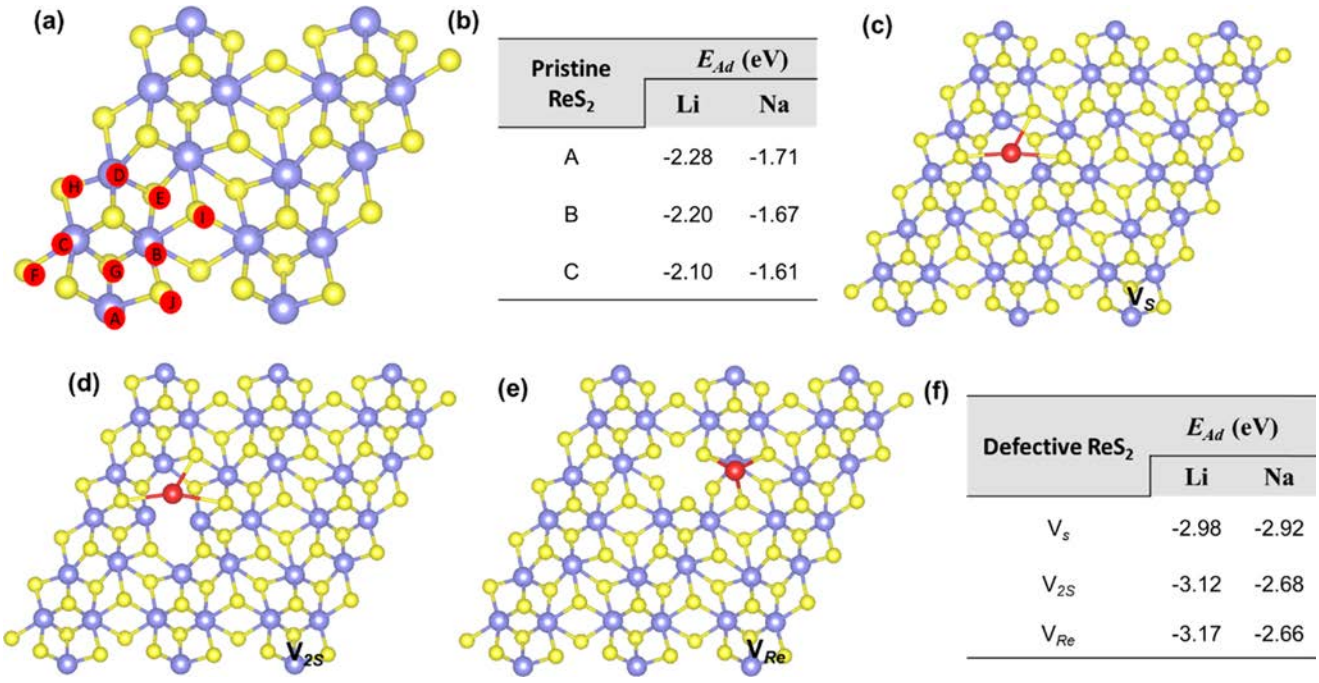

Pristine ReS_2	E_{Ad} (eV)	
	Li	Na
A	-2.28	-1.71
B	-2.20	-1.67
C	-2.10	-1.61

Defective ReS_2	E_{Ad} (eV)	
	Li	Na
V_s	-2.98	-2.92
V_{2S}	-3.12	-2.68
V_{Re}	-3.17	-2.66

Figure 2. (a) Top view of the most stable sites for the adsorption of Li and Na over monolayer pristine ReS_2. (b) Comparison of adsorption energies of Li and Na over pristine ReS_2 for three most favorable active sites. Most stable sites for Li and Na adsorption over (c) V_S, (d) V_{2S}, and (e) V_{Re}. Color code for atoms: yellow, S; violet, Re; red, Li and Na. (f) Adsorption energies of Li and Na over V_S, V_{2S}, and V_{Re}.

point defects in anisotropic ReS_2 are distinct from those in isotropic binary honeycomb-like TMDs, such as MoS_2 and VS_2.[39] For example, using high-resolution transmission electron microscopy and Raman spectroscopy, Wu et al.[29] identified and characterized the grain boundary structure in ReS_2 nanofilms and demonstrated that a variety of clusters and single, double, and triple vacancies are formed, which are complex in comparison to defect structures reported for other 2D systems.

Commonly observed point defects in ReS_2 are monosulfur vacancy (V_S), disulfur vacancy (V_{2S}), and single-metal vacancy (V_{Re}). Horzum et al.[39] systematically studied the energetics of different point defects in ReS_2 and found that the stability of the defects are site-dependent. They reported that the most stable single S vacancy in ReS_2 is obtained by removing a S atom from ReS chains (Figure 1c). The most stable V_{2S} is created by removing two S atoms from the same sublattice, i.e., by removing another S atom neighboring the V_S (Figure 1d). Although two possible sites exist for creating V_{Re}, the one with the lowest formation energy is shown in Figure 1e. The relative stability of different point defects in a system is determined in terms of the formation energy of the defect, which is given by

$$E_f = E_{def} - E_{pristine} + \sum_i N\mu_i \quad (6)$$

where E_{def} and $E_{pristine}$ are the total energies of the defective and pristine supercells, N is the number of ith atoms removed from the pristine surfaces to create defects, and μ_i is the chemical potential of the ith species in its stable bulk form. Under thermal equilibrium, the chemical potential of ReS_2 monolayer satisfies $\mu_{ReS_2} = \mu_{Re} + 2\mu_S$, where μ_{Re} and μ_S are the chemical potentials for Re and S, respectively. For a Re-rich environment, $\mu_{Re} = E_{tot}(Re)$, where $E_{tot}(Re)$ is the total energy of a Re atom in the bulk form. Thus, $\mu_S = (\mu_{ReS_2} - \mu_{Re})/2$. Under S-rich condition, $\mu_S = E_{tot}(S)$, where $E_{tot}(S)$ is the energy of a S atom in the bulk form. Therefore, μ_{Re} can be calculated as $\mu_{Re} = \mu_{ReS_2} - 2\mu_S$. The formation energies for V_S, V_{2S}, and V_{Re} are 1.18, 2.61, and 4.9 eV under S-rich conditions and 2.14, 4.53, and 3.02 eV under Re-rich condition, respectively (Figure 1f). These magnitudes of formation energies agree with those reported in ref 39. The formation energy of V_S is the lowest under both Re-rich and S-rich conditions, which suggests that sulfur single vacancies are most likely to form during mechanical exfoliation. This behavior is similar to MoS_2, in which V_S is the most energetically favored point defect but is unlike graphene, wherein carbon double vacancy is the most favored point defect. Also, since the formation energy of V_{2S} is larger than twice that of V_S, two separate V_S would not combine to create a disulfur V_{2S} vacancy. Additionally, the Re single vacancy has the largest formation energy compared to V_S even under a S-rich condition. At a finite temperature, T, the areal density of defects is related to the formation energy of the defect and can be calculated using an Arrhenius-type equation given by

$$N_{defect} = N_{pristine} \exp\left(-\frac{E_f^T}{k_B T}\right) \quad (7)$$

where $N_{pristine}$ is the areal density of atoms in the pristine material, E_f^T is the formation energy of the defect at T, k_B is the Boltzmann constant. Temperature-dependent magnitudes of E_f^T can be calculated by performing ab initio molecular dynamics simulations.

3.2. Adsorption of Li and Na on Pristine and Defective ReS_2. Pristine ReS_2 is anisotropic, which gives rise to several asymmetric adsorption sites favorable for lithiation and sodiation. The binding energies for the adsorption of Li and Na atoms for a set of 10 active sites over monolayer pristine ReS_2 surface have been evaluated. The equilibrium positions for Li and Na atoms were determined by first placing the adatoms 3.5 Å away from the ReS_2 surface and subsequently optimizing

DOI: 10.1021/acsami.7b13604
ACS Appl. Mater. Interfaces 2018, 10, 5373−5384

the structure by minimizing the overall energy. DFT calculations show that site-A with E_{ad} = −2.28 eV for Li and −1.71 eV for Na is the most favorable location for both lithiation and sodiation over pristine ReS_2. The metal atoms prefer to reside near the area in between three sulfur atoms. For the adsorption of Li over site-B and site-C, the magnitudes of E_{ad} are −2.2 and −2.1 eV, respectively. The adsorption energy of Li over site-A is 0.89 eV higher than that of SnS_2,[14] 0.26 eV higher than that of GeS,[50] 0.1 eV higher than that of MoS_2.[35] Similarly, the adsorption energy of Na over site-A is 1.3 eV higher than that of pentagraphene,[51] 0.35 eV higher than that of GeS,[50] and 0.2 eV higher than that of Ti_3C_4.[52] The adsorption energies for Na over site-B and site-C are −1.67 and −1.61 eV, respectively. Equilibrium configurations and binding energies of Li and Na adsorption over site-A, site-B, and site-C are also presented in Figure 2a,b, with the corresponding charge density difference contours presented in Figures S1 and S2. The binding energies of Li and Na over all of the 10 sites are presented in Table S2. Negative adsorption energies for a range of adsorption sites indicate that Li and Na storage over pristine ReS_2 is a spontaneous process, which is an essential requirement for alkali-metal-ion batteries. Also, the binding energy associated with the adsorption of Li and Na is the largest near the Re chains. Thus, the adatoms atoms tend to accumulate near these Re chains.

Previous studies of Li adsorption on 2D materials suggest that metal adatoms tend to get adsorbed adjacent to the defective zone because of the unused electrons from the dangling bonds.[37,38] To find the best adsorption sites for Li and Na onto defective ReS_2, a host of initial positions for the adatoms were considered around the defective sites, the strongest adsorption sites, and the corresponding adsorption energies are shown in Figure 2c−f. On defective ReS_2, Li and Na atoms prefer to get adsorbed in the hollow site between two S atoms. For example, in the case of V_S (Figure 2c), both Li and Na prefer to bind directly over the vacancy, suggesting it has taken the place of the sulfur atom. The binding energies for Li and Na over V_S are 2.98 and 2.92 eV, respectively. In the case of V_{2S} (Figure 2d), the metal atoms prefer to adsorb onto a similar position, with binding energies of −3.12 and 2.68 eV for Li and Na, respectively. The adsorption of a Li atom over monolayer ReS_2 with a V_{Re} (Figure 2e) is the strongest with a binding energy of −3.17 eV, compared to a binding energy of −2.28 eV for pristine ReS_2. However, in the case of V_{Re}, the metal atoms tend to get adsorbed over site-A close to V_{Re} rather than the hollow site created by the vacancy. Binding energies, the shortest distance between the adsorbent atoms and the Re and S atoms in pristine and defective ReS_2 are presented in Table 1. Charge density difference contours for Li and Na adsorption over defective ReS_2 are presented in Figures S3 and S4.

Table 1. Adsorption Energies (E_{ad}), the Shortest Distance between Li Atom at Neighboring Re Atom (d_{Li-Re}) and S Atom (d_{Li-S}) for Pristine, V_S, V_{2S}, and V_{Re} Monolayer ReS_2

E_{ad} (eV)	adsorbent	pristine	V_S	V_{2S}	V_{Re}
	Li	2.28	2.98	3.12	3.17
	Na	1.71	2.92	2.68	2.66
d_{Li-Re} (Å)	Li	2.95	2.78	2.73	2.89
	Na	2.93	3.14	3.07	3.46
d_{Li-S} (Å)	Li	2.26	2.59	2.48	2.30
	Na	3.96	2.82	2.77	2.71

Additionally, Bader charge analysis[53] was conducted to quantify the charge-transfer process and understand the nature of interaction between the substrate (pristine and defective) and the adatoms, the details of which are presented in Figure S5.

To better understand the adsorption mechanism and ensure that the ideal electrode characteristics of ReS_2 are retained, the projected density of states (PDOS) of all bound systems were calculated, as shown in Figure 3. As Li and Na atoms adsorb over pristine, and defective ReS_2 monolayers, they provide some electronic states to each system and act as electron-donor species. The Li and Na 2s states are found deep in the conduction band, in all ReS_2 systems, at energy levels corresponding to the magnitude of their respective binding energies. The adsorption of Li and Na in turn pushes the Fermi level to higher energies, n-doping all of the ReS_2 systems. After the adsorption of Li and Na, the Fermi levels of pristine, V_S, and V_{2S} ReS_2 monolayers are found at the bottom of the conduction band, increasing the free-electron concentration, giving rise to n-type semiconducting monolayers. The adsorption of Na on the pristine ReS_2 monolayer also closes the band gap between the valence and conduction bands, decreasing it to ∼0.6 eV. After the adsorption of Li and Na on the V_{Re} ReS_2 monolayer, the Fermi level is found at the top of valence band. The adsorption of Li and Na atoms decreases the conducting hole concentration, due to the n-doping, pushing the Fermi level to higher energies. However, at higher Li and Na concentrations, the Fermi level can be expected to increase to the bottom of the conduction band, creating an n-type semiconducting monolayer, increasing the free-electron concentration. The increase in free-electron concentration in all ReS_2 monolayer systems may increase their electrical conductivity and potentially enhance their electrode performance.

Throughout the charging/discharging process, the concentration of the metallic ions in alkali-metal-ion batteries changes, resulting in compositional changes. Depending on the concentration of the alkali atoms, the adsorption sites vary, which is why it is important to study the effect of composition on the adsorption over pristine monolayer ReS_2. Additionally, for commercial purposes, the OCV is widely used for characterizing the performance of alkali-metal-ion batteries, such as the state of charge and health. OCV can be evaluated by estimating the voltage for a range of metal atoms stoichiometry. Here, to find E_{avg}, OCV, and specific capacity of pristine ReS_2 as a function of Li and Na concentration, a 2 × 2 supercell (16 Re atoms, 32 S atoms) is considered. Simulations were performed for a range of initial arrangements of Li and Na atoms. Initially, the adatoms were placed over site-A, site-B, or site-C, away from each other to avoid interactions of the adsorbent atoms. All of the structures are then fully optimized. The alkali atoms can be adsorbed until the average binding energy of each Li atom reaches 0 eV; however, for larger concentrations of the alkali atoms, the Re−S bonds may become weak or can fail, and they cannot rebuild and the charging/discharging process becomes irreversible. Therefore, low alkali atom concentrations have been considered here. Different compositions of Li_xReS_2 and Na_xReS_2 were studied with x taking on values of 0.125 0.25, 0.375, 0.5, 1, 1.25, 1.5, 2, 2.5, and 4. Simulations show that the electrostatic repulsive force between the metal atoms increases progressively as the number of adatoms is increased. This leads to increasingly weaker adsorption. The highest Li/Na concentration is a 4:1 ratio between the adatoms and ReS_2 (i.e., Li_4ReS_2 and Na_4ReS_2), which leads to a specific capacity of

DOI: 10.1021/acsami.7b13604
ACS Appl. Mater. Interfaces 2018, 10, 5373−5384

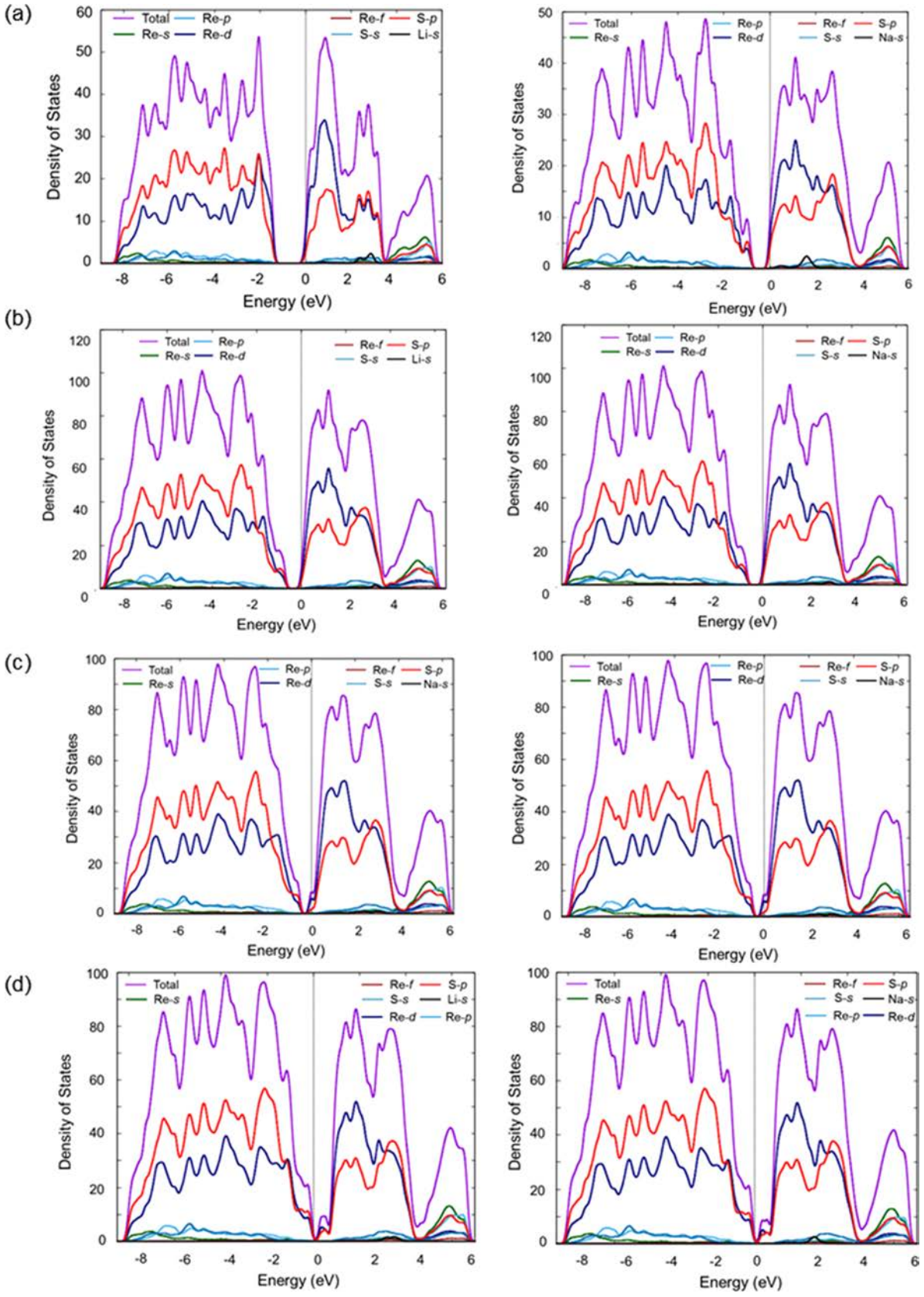

Figure 3. (Left) Projected density of states (PDOS) of the Li bound to (a) pristine, (b) V_S, (c) V_{2S}, and (d) V_{Re} ReS_2 systems. (Right) PDOS of the Na bound to (a) pristine, (b) V_S, (c) V_{2S}, and (d) V_{Re} systems. The Fermi energies for all plots were set to 0 eV.

428 mAh/g for both Li and Na. The average adsorption energies (E_{avg}) are −0.43 and −0.55 eV for Li and Na, respectively. When extra metal atoms are added over the substrate, they are either pushed away from the ReS_2 surface or

DOI: 10.1021/acsami.7b13604
ACS Appl. Mater. Interfaces 2018, 10, 5373−5384

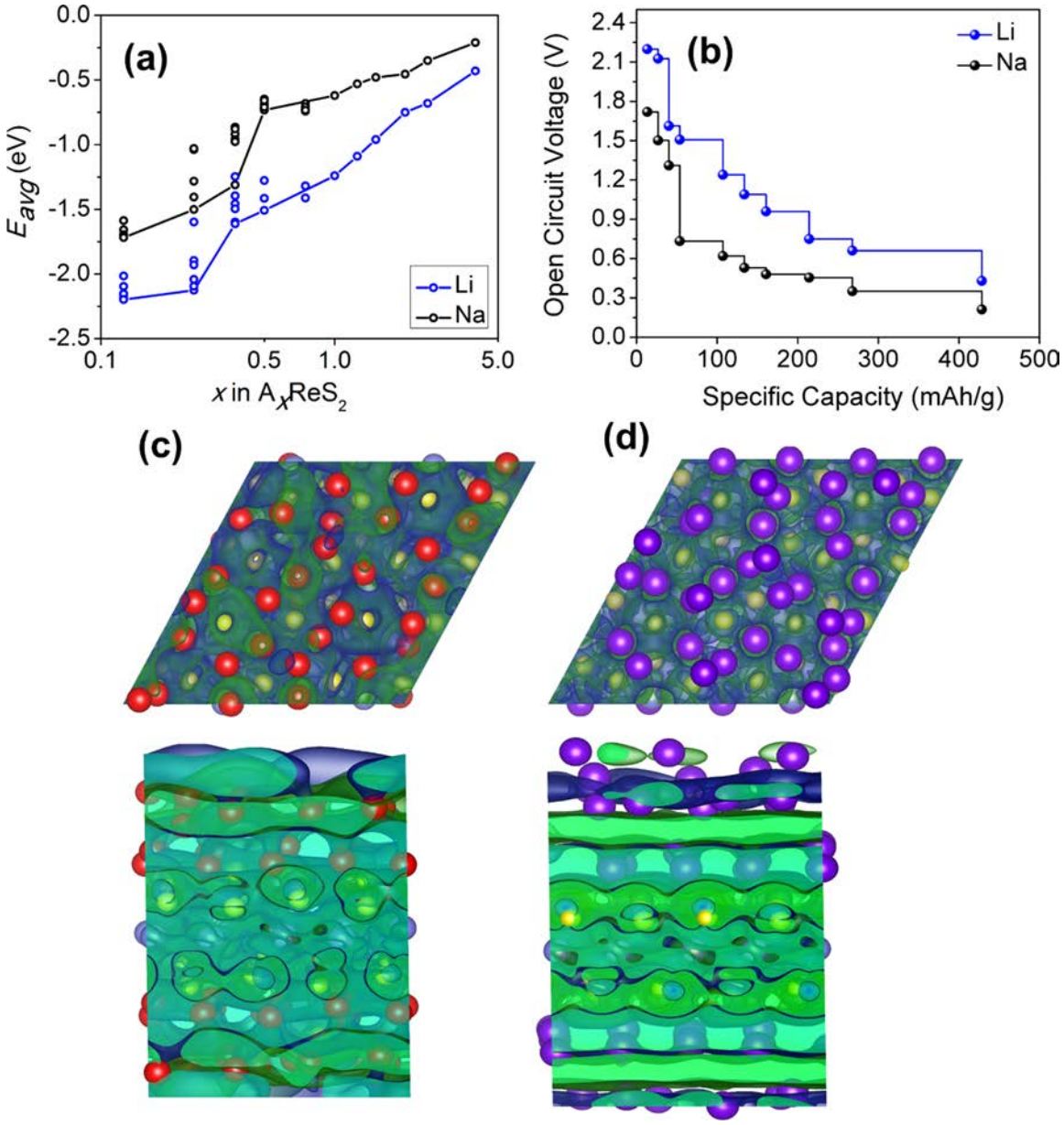

Figure 4. (a) Average adsorption energy as a function of Li/Na adsorption concentration. (b) Open-circuit voltage for Li/Na adatoms as a function of specific capacity. Top view and side view of charge density difference plots for (c) Li_4ReS_2 and (d) Na_4ReS_2. Color code for atoms: yellow, S; blue, Re; red, Li; violet, Na. The isosurface level is set to be 0.0002 e/A^3. Green and light blue regions indicate charge accumulation and depletion, respectively.

the substrate experiences irreparable distortion. The open-circuit voltages as a function of specific capacity for Li and Na are shown in Figure 4a,b. It can be noted that the voltage profiles of ReS_2 for increasing concentrations of Li and Na are similar to those of graphene,[34,38] 2D MoS_2, VS_2 nanocomposite,[47] Ti_3C_2,[48] GeS,[50] and other 2D materials,[13,54] and the low values indicate its suitability as an anode material in both cases. The charge density difference plots for Li_4ReS_2 and Na_4ReS_2 are shown in Figure 4c,d. The specific capacity of 428 mAh/g is in excellent agreement with 427 mAh/g measured experimentally by Qi et al.[22] Additionally, they demonstrated that the capacity of bare ReS_2 can be further improved to 1048 mAh/g with a high capacity retention of 93.6% after 100 cycles by creating a ReS_2- and carbon nanotube-based composite. Additionally, although the specific capacity of ReS_2 for Li intercalation is better than that of monolayer GeS (256 mAh/g), the specific capacity of 428 mAh/g for Na is poorer than GeS (512 mAh/g).[50]

3.3. Diffusion of Li and Na on Pristine and Defective ReS_2 Surface. The performance of the anode material in alkali-metal-ion batteries is determined by the competition between adsorption and diffusion of ions over substrate. From a purely thermodynamic standpoint, the alkali atoms would want to migrate from the most favorable adsorption site of one unit cell to their counterparts in the neighboring unit cells. It is well known that the charging/discharging rate depends on the mobility of alkali ions in the anode of the battery. In most 2D materials, such as MoS_2, graphene, phosphorene, and metallic carbides, the overall structure is highly symmetric and a small diffusion pathway is representative of the overall diffusion pathways in the material. In ReS_2, however, the structural anisotropy and lack of symmetry create more unique pathways

DOI: 10.1021/acsami.7b13604
ACS Appl. Mater. Interfaces 2018, 10, 5373−5384

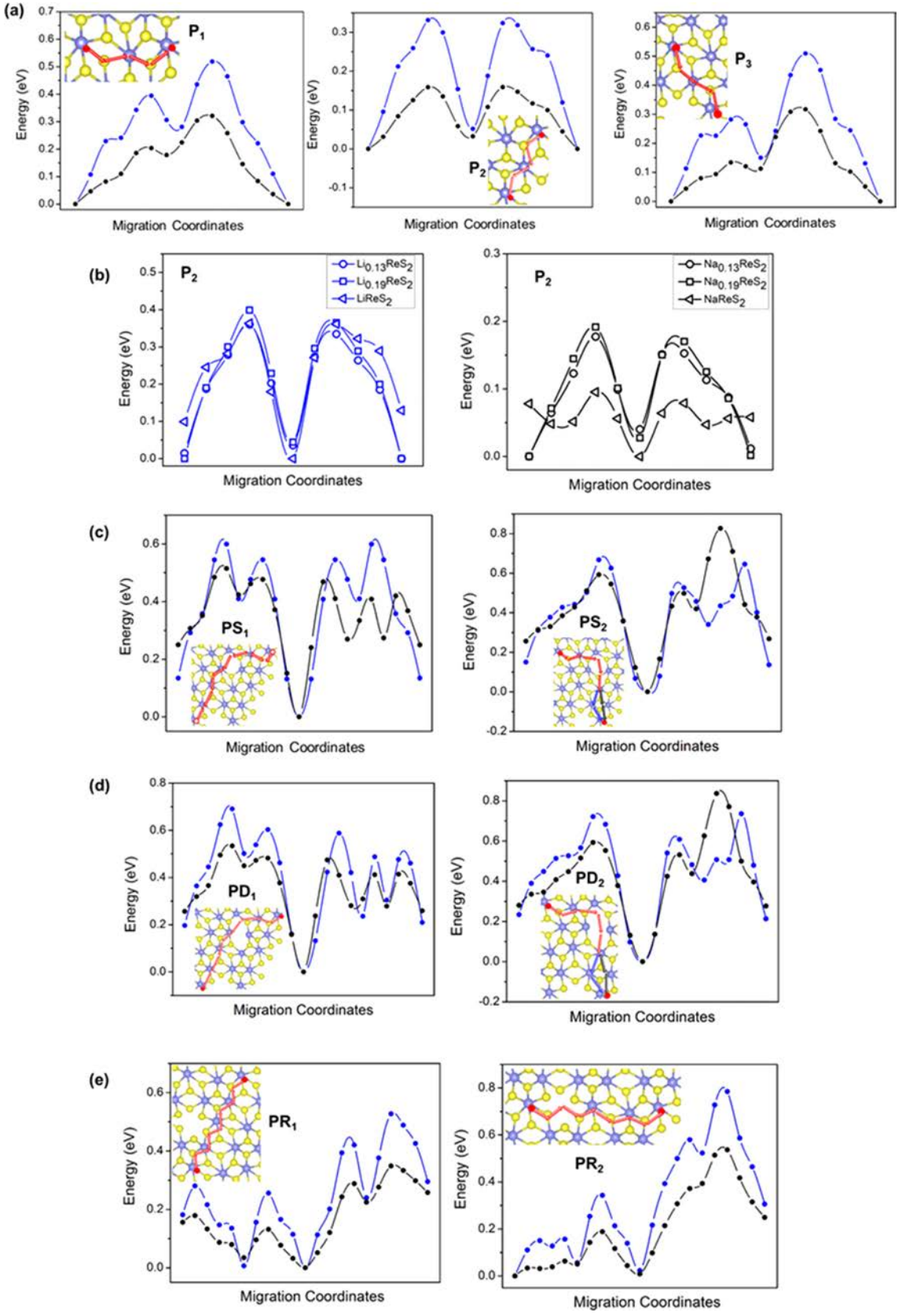

Figure 5. Diffusion of Li (blue) and Na (black) over pristine and defective ReS_2. Energy profile associated with the diffusion of (a) one isolated Li atom and one isolated Na atom over pristine ReS_2, (b) a range of concentrations of Li and Na over pristine ReS_2, one isolated Li atom and one isolated Na atom over, (c) V_S, (d) V_{2S}, and (e) V_{Re}. The red circles represent initial and final positions of the diffusing atoms used for the NEB calculations. The arrows in the insets show the mean energy pathways (MEPs) of diffusing atoms. The red arrows represent the common migration path for both Li and Na atoms, whereas the blue and black arrows represent individual paths for Li and Na when they are not identical.

DOI: 10.1021/acsami.7b13604
ACS Appl. Mater. Interfaces 2018, 10, 5373−5384

for diffusion to occur. Essentially, Li and Na ions can diffuse over Re chains and S chains. Therefore, from a kinetics standpoint, to accurately find the most favored diffusion pathways and the associated activation energy barriers (E_a), we simulated longer diffusion pathways.

Here, the energy barriers associated with the diffusion of Li atoms over pristine and defective ReS_2 monolayers are reported. For pristine ReS_2, diffusion of Li and Na atoms was considered in three different directions, i.e., NEB simulations were performed to find the energy barriers associated with the migration of a Li and a Na atom from site-A to their counterparts in neighboring unit cells in a 2 × 2 supercell. Schematics of the minimum-energy pathways (MEPs) and corresponding energy barriers as a function of diffusion paths are plotted in Figure 4a. Similarly, the MEPs and the energy barriers for the diffusion of Li from site-B are presented in Figure S6. For Li, the diffusion barrier for path P_2 is 0.33 eV, whereas for both P_2 and P_3, the value is 0.51 eV. These numbers are in excellent agreement with an energy barrier of 0.39 eV for Li diffusion in pristine ReS_2 reported earlier.[23] On the other hand, for Na diffusion, the magnitudes of E_a for paths P_1, P_2, and P_3 are 0.31, 0.16, and 0.32 eV, respectively. The difference in the binding energy between site-A and site-B is merely 0.1 eV for Li and 0.04 eV for Na, causing a similar adsorption energy along the furrows and smaller diffusion energy barrier for path P_2. It is obvious that the diffusion of a Li atom on perfect ReS_2 is not isotropic, which is due to the inherent lack of structural and electronic symmetry. However, because the energy barrier for P_2 is the smallest (path length ∼6 Å), 0.33 and 0.16 eV are the energy barriers for the diffusion of Li and Na over pristine ReS_2, respectively. To give these numbers some perspective, the diffusion barriers of Li over graphene, phosphorene, MoS_2, flat borophene, GeS, and Ti_3C_2 MXene are 0.37,[55] 0.13−0.76,[56] 0.24,[35] 0.69,[57] 0.24,[50] and 0.7 eV,[48] respectively. Similarly, the barrier heights for Na diffusion over graphene, flat borophene, GeS, and phosphorene are 0.19,[37] 0.34,[57] 0.09,[50] and 0.04 eV,[58] respectively. Low energy barriers for Li and Na diffusion over pristine ReS_2 indicates its fast charge−discharge capabilities for AIBs.

To find the effect of adatom concentration on the diffusion, we performed CI-NEB simulations for three other concentrations of Li and Na. Because P_2 was earlier found to be the lowest energy diffusion pathway, these additional simulations were therefore performed for the same pathway. Associated energy profiles are shown in Figure 4b. The compositions of the systems were $A_{0.13}ReS_2$, $A_{0.19}ReS_2$, and $AReS_2$, where A = Li and Na. The results from our simulations are interesting. Initially, as the adatom concentration is increased, the energy barriers slightly increase for both Li and Na. For example, the energy barriers for $Li_{0.13}ReS_2$ and $Li_{0.19}ReS_2$ are 0.36 and 0.39 eV, respectively, compared to the energy barrier of 0.33 eV for the system $Li_{0.0625}ReS_2$. Similarly, for $Na_{0.13}ReS_2$ and $Na_{0.19}ReS_2$, the energy barriers to diffusion are 0.17 and 0.19 eV, respectively, compared to the energy barrier of 0.16 eV for the $Na_{0.0625}ReS_2$. Interestingly, as the concentration of Li/Na is increased further, while the energy barrier for Li diffusion remains unchanged, the barrier for Na diffusion reduces dramatically. For example, the barrier for Li diffusion in the system $LiReS_2$ is only 0.36 eV; however, the barrier to Na diffusion is a meager 0.09 eV in $NaReS_2$. These results indicate that for an LIB containing ReS_2 as anode material, the rate of charging/discharging will not change with increasing concentrations of Li, but the rate will increase considerably with Na concentration in ReS_2-based NIBs.

Although strong adsorption energies achieved by the introduction of lattice defects are desirable for the alkali atom in anode materials, too high of a binding energy can inhibit the atomic motion and diffusion. With large adsorption energies, the defective sites sometimes essentially act as traps and consequently the associated diffusion barriers can increase sharply. For defective ReS_2, we have simulated the entire diffusion pathways, including confinement of the alkali atoms in the vicinity of the defective sites and their escape from the defective regions. Our NEB simulations of minimum-energy pathways for Li and Na diffusion suggest that V_S, V_{2S}, and V_{Re} trap the alkali-metal atoms to different degrees and as a result increase the diffusion energy barriers compared to the defect-free case. As shown before, V_S is the most probable point defect to form in monolayer ReS_2 under both Re- and S-rich conditions. Therefore, the effect of V_S on diffusion is discussed first. Similar to pristine ReS_2, for V_S also, two distinct migration paths across the defective site have been considered. The energy barriers for escaping the defective site are relatively larger than that of pristine ReS_2. As shown in Figure 4c, the diffusion barrier increases to 0.55 eV for Li and 0.47 eV for Na, as the alkali atoms migrate along path PS_1 escaping V_S, whereas it increases to 0.67 eV for Li and 0.59 eV for Na along PS_2. Similarly, for V_{2S} (Figure 4d), we considered two migration paths, namely, PD_1 and PD_2. As shown in Figure 4d, the energy barriers for diffusion along PD_1 and PD_2 were 0.72 and 0.6 eV for Li and 0.59 and 0.48 eV for Na, respectively. It is noteworthy that the diffusion energy barrier is comparatively small in the vicinity of the defect, whereas it is significantly large when escaping the defective site. This effect has been observed before in defective monolayer black phosphorus.[38] Finally, for V_{Re} (Figure 5e), two diffusion paths were considered, namely, path PR_1 and PR_2. The diffusion barrier for path PR_1 increases to 0.42 eV for Li and 0.28 eV for Na. On the other hand, for path PR_2, the energy barrier increases to 0.58 eV for Li and 0.54 eV for Na. Therefore, the largest increase in the energy barrier takes place when traversing a double vacancy, whereas the lowest increase in energy barrier happens near a Re single vacancy. From these values of migration energy barriers, it is evident that the diffusion of Li and Na atoms are difficult in defective ReS_2 monolayers compared to pristine ReS_2. A summary of diffusion energy barriers for the migration of Li and Na over pristine, V_S, V_{2S}, and V_{Re} ReS_2 is presented in Table 2.

Table 2. Summary of Diffusion Energy Barriers for the Migration of Li and Na over Pristine, V_S, V_{2S}, and V_{Re} ReS_2

	diffusion energy barrier (eV)			
alkali metal	pristine	V_S	V_{2S}	V_{Re}
Li	0.33	0.55	0.60	0.42
Na	0.16	0.47	0.48	0.28

According to Arrhenius equation, the diffusion constant (D) is given by

$$D \sim \exp\left(\frac{-E_a}{k_B T}\right) \quad (8)$$

where k_B is the Boltzmann constant and T is the operating temperature. The following predictions can be made using eq 8 (a) The diffusion of Na over pristine ReS_2 is 700 times faster

DOI: 10.1021/acsami.7b13604
ACS Appl. Mater. Interfaces 2018, 10, 5373−5384

than that of Li. (b) Although the presence of V_{Re} in pristine monolayer ReS_2 reduces the diffusivity of Li atoms by a mere 32 times, the introduction of V_S and V_{2S} slows it down by 5.3×10^3 and 3.6×10^3 times. In case of Na, the diffusion over V_{Re}, V_S, and V_{2S} can be 1.06×10^2, 1.7×10^5, and 2.6×10^5 times slower than pristine ReS_2, respectively. These results indicate that Li and Na atoms tend to migrate to the defective sites, and as a result, the energy barriers associated with the backward migration increase. Also, the presence of V_{Re} reduces the charging/discharging rates of ReS_2-based AIBs marginally, whereas the adsorption capacity of the ReS_2 monolayer improves considerably. Although the introduction of V_S and V_{2S} defects increases the binding energy of Li atoms, they significantly reduce the diffusion rates of the atoms, especially in case of Na diffusion. Therefore, it is desirable to avoid their formation to retain the advantages of ReS_2 for AIBs applications. These observations are contrary to those for V_S and V_{2S} containing MoS_2, wherein the effect of point defects on the energy barriers for Li diffusion is negligible. The concentrations of V_S and V_{2S} can be reduced by increasing their formation energies. Therefore, an increase in the chemical potential of S in the surrounding environment during the ReS_2 fabrication process (CVD) could reduce the concentrations of V_S and V_{2S}. Similarly, a reduction in the concentration of Re in the surrounding should also facilitate the formation of Re single vacancy and discourage the formation of S-based defects. Additionally, research done on MoS_2 monolayers shows that S atoms containing thiol-group-containing molecules get adsorbed at the S-vacancy sites post-treatment, resulting in the reinsertion of missing sulfur atom.[59,60] As a result of this treatment, disulfides are formed on the MoS_2, thereby alleviating the detrimental effects of S-based point defects. In conclusion, the presence of V_{Re} enhances the capacity of the ReS_2-based AIBs, without affecting their charging/discharging rates and hence is not detrimental to their battery performance.

4. CONCLUSIONS

Single-layer rhenium disulfide is a unique material with distinctive, anisotropic electronic, mechanical, and optical properties and has the potential to be used as an anode material in alkali-metal-ion batteries. By performing density functional theory calculations, we have analyzed the adsorption and diffusional characteristics of two alkali metals, namely, Li and Na, on pristine and defective monolayer ReS_2. Our studies show that Li and Na atoms can be adsorbed over pristine ReS_2 with binding energies of −2.28 and −1.71 eV, respectively, with several other potential adsorption sites for both. The diffusion of Li and Na over pristine ReS_2 is anisotropic, with energy barriers of 0.33 and 0.16 eV, respectively. The energy barriers associated with escaping a S double vacancy and single vacancy are significantly large, 0.6 and 0.51 eV for Li and 0.59 and 0.47 eV for Na, which indicates slower migration and sluggish charging/discharging (by a factor of 10^3−10^5 compared to pristine ReS_2). However, the diffusion energy barrier over Re single vacancy was found to be merely 0.42 eV for Li and only 0.28 eV for Na. These results suggest that monolayer ReS_2 with Re single vacancy adsorbs both Li and Na stronger than pristine ReS_2, with negligible negotiation with the charging/discharging rate of the battery, and therefore can be a suitable anode material. In fact, a proper combination of defects and topological disorders can generate more energetically favorable structures and provide ways for more efficient battery technologies.

■ ASSOCIATED CONTENT

Supporting Information

The Supporting Information is available free of charge on the ACS Publications website at DOI: 10.1021/acsami.7b13604.

Adsorption energy of Li/Na with vacuum, adsorption energy of Li/Na over pristine ReS_2, differential charge density plots, Bader charge analysis for Li/Na adsorption over pristine and defective ReS_2, and diffusion of Li over site-B (PDF)

■ AUTHOR INFORMATION

Corresponding Author

*E-mail: chandraveer.singh@utoronto.ca.

ORCID

Nikhil Koratkar: 0000-0002-4080-3786

Chandra Veer Singh: 0000-0002-6644-0178

Author Contributions

All of the authors contributed toward preparing the manuscript and have given approval to the current version.

Notes

The authors declare no competing financial interest.

■ ACKNOWLEDGMENTS

The authors acknowledge funding by the Natural Sciences and Engineering Research Council of Canada (NSERC) through the Discovery Grant, undergraduate scholarship programs, the Hart Professorship, and the University of Toronto. The authors also acknowledge Compute Canada for providing computing resources at the SciNet CalculQuebec, and Westgrid consortia. The authors thank Lance Kavalsky for help with electronic structure calculations and Hao Sun for important discussions.

■ REFERENCES

(1) Idota, Y.; Kubota, T.; Matsufuji, A.; Maekawa, Y.; Miyasaka, T. Tin-Based Amorphous Oxide: A High-Capacity Lithium-Ion-Storage Material. *Science* **1997**, *276*, 1395−1397.

(2) Yoo, E.; Kim, J.; Hosono, E.; Zhou, H.-s.; Kudo, T.; Honma, I. Large Reversible Li Storage of Graphene Nanosheet Families for Use in Rechargeable Lithium Ion Batteries. *Nano Lett.* **2008**, *8*, 2277−2282.

(3) Ji, L.; Lin, Z.; Alcoutlabi, M.; Zhang, X. Recent developments in nanostructured anode materials for rechargeable lithium-ion batteries. *Energy Environ. Sci.* **2011**, *4*, 2682−2699.

(4) Chen, K.; Xue, D. Materials chemistry toward electrochemical energy storage. *J. Mater. Chem. A* **2016**, *4*, 7522−7537.

(5) Hwang, J.-Y.; Myung, S.-T.; Sun, Y.-K. Sodium-ion batteries: present and future. *Chem. Soc. Rev.* **2017**, *46*, 3529−3614.

(6) Deng, D. Li-ion batteries: basics, progress, and challenges. *Energy Sci. Eng.* **2015**, *3*, 385−418.

(7) Wang, G.; Shen, X.; Yao, J.; Park, J. Graphene nanosheets for enhanced lithium storage in lithium ion batteries. *Carbon* **2009**, *47*, 2049−2053.

(8) Yang, S.; Li, S.; Tang, S.; Dong, W.; Sun, W.; Shen, D.; Wang, M. Sodium adsorption and intercalation in bilayer graphene from density functional theory calculations. *Theor. Chem. Acc.* **2016**, *135*, 164.

(9) Zhong, H.-X.; Gao, S.; Shi, J.-J.; Yang, L. Quasiparticle band gaps, excitonic effects, and anisotropic optical properties of the monolayer distorted 1 T diamond-chain structures ReS_2 and $ReSe_2$. *Phys. Rev. B* **2015**, *92*, No. 115438.

(10) Zhao, S.; Kang, W.; Xue, J. The potential application of phosphorene as an anode material in Li-ion batteries. *J. Mater. Chem. A* **2014**, *2*, 19046−19052.

DOI: 10.1021/acsami.7b13604
ACS Appl. Mater. Interfaces 2018, 10, 5373−5384

(11) Kulish, V. V.; Malyi, O. I.; Persson, C.; Wu, P. Phosphorene as an anode material for Na-ion batteries: a first-principles study. *Phys. Chem. Chem. Phys.* **2015**, *17*, 13921−13928.
(12) Jiang, H. R.; Lu, Z.; Wu, M. C.; Ciucci, F.; Zhao, T. S. Borophene: A promising anode material offering high specific capacity and high rate capability for lithium-ion batteries. *Nano Energy* **2016**, *23*, 97−104.
(13) Rao, D.; Zhang, L.; Meng, Z.; Zhang, X.; Wang, Y.; Qiao, G.; Shen, X.; Xia, H.; Liu, J.; Lu, R. Ultrahigh energy storage and ultrafast ion diffusion in borophene-based anodes for rechargeable metal ion batteries. *J. Mater. Chem. A* **2017**, *5*, 2328−2338.
(14) Tu, K.; Li, F.; Chen, Z. Enhanced lithium adsorption/diffusion and improved Li capacity on SnS_2 nanoribbons: A computational investigation. *J. Mater. Res.* **2016**, *31*, 878−885.
(15) Li, Y.; Wu, D.; Zhou, Z.; Cabrera, C. R.; Chen, Z. Enhanced Li Adsorption and Diffusion on MoS_2 Zigzag Nanoribbons by Edge Effects: A Computational Study. *J. Phys. Chem. Lett.* **2012**, *3*, 2221−2227.
(16) Stephenson, T.; Li, Z.; Olsen, B.; Mitlin, D. Lithium ion battery applications of molybdenum disulfide (MoS_2) nanocomposites. *Energy Environ. Sci.* **2014**, *7*, 209−231.
(17) Liu, Y.; Wang, W.; Wang, Y.; Peng, X. Homogeneously assembling like-charged WS_2 and GO nanosheets lamellar composite films by filtration for highly efficient lithium ion batteries. *Nano Energy* **2014**, *7*, 25−32.
(18) Aslan, O. B.; Chenet, D. A.; van der Zande, A. M.; Hone, J. C.; Heinz, T. F. Linearly Polarized Excitons in Single- and Few-Layer ReS_2 Crystals. *ACS Photonics* **2016**, *3*, 96−101.
(19) Cao, C.; Daly, M.; Chen, B.; Howe, J. Y.; Singh, C. V.; Filleter, T.; Sun, Y. Strengthening in graphene oxide nanosheets: bridging the gap between interplanar and intraplanar fracture. *Nano Lett.* **2015**, *15*, 6528−6534.
(20) Tongay, S.; Sahin, H.; Ko, C.; Luce, A.; Fan, W.; Liu, K.; Zhou, J.; Huang, Y.-S.; Ho, C.-H.; Yan, J.; et al. Monolayer behaviour in bulk ReS_2 due to electronic and vibrational decoupling. *Nat. Commun.* **2014**, *5*, No. 3252.
(21) Shi, F.; Song, Z.; Ross, P. N.; Somorjai, G. A.; Ritchie, R. O.; Komvopoulos, K. Failure mechanisms of single-crystal silicon electrodes in lithium-ion batteries. *Nat. Commun.* **2016**, *7*, No. 11886.
(22) Qi, F.; He, J.; Chen, Y.; Zheng, B.; Li, Q.; Wang, X.; Yu, B.; Lin, J.; Zhou, J.; Li, P.; Zhang, W.; Li, Y. Few-layered ReS_2 nanosheets grown on carbon nanotubes: A highly efficient anode for high-performance lithium-ion batteries. *Chem. Eng. J.* **2017**, *315*, 10−17.
(23) Zhang, Q.; Tan, S.; Mendes, R. G.; Sun, Z.; Chen, Y.; Kong, X.; Xue, Y.; Rümmeli, M. H.; Wu, X.; Chen, S.; Fu, L. Extremely Weak van der Waals Coupling in Vertical ReS_2 Nanowalls for High-Current-Density Lithium-Ion Batteries. *Adv. Mater.* **2016**, *28*, 2616−2623.
(24) Gao, J.; Li, L.; Tan, J.; Sun, H.; Li, B.; Idrobo, J. C.; Singh, C. V.; Lu, T.-M.; Koratkar, N. Vertically Oriented Arrays of ReS_2 Nanosheets for Electrochemical Energy Storage and Electrocatalysis. *Nano Lett.* **2016**, *16*, 3780−3787.
(25) Chenet, D. A.; Aslan, O. B.; Huang, P. Y.; Fan, C.; van der Zande, A. M.; Heinz, T. F.; Hone, J. C. In-Plane Anisotropy in Mono- and Few-Layer ReS_2 Probed by Raman Spectroscopy and Scanning Transmission Electron Microscopy. *Nano Lett.* **2015**, *15*, 5667−5672.
(26) Pradhan, N. R.; McCreary, A.; Rhodes, D.; Lu, Z.; Feng, S.; Manousakis, E.; Smirnov, D.; Namburu, R.; Dubey, M.; Hight Walker, A. R.; Terrones, H.; Terrones, M.; Dobrosavljevic, V.; Balicas, L. Metal to Insulator Quantum-Phase Transition in Few-Layered ReS_2. *Nano Lett.* **2015**, *15*, 8377−8384.
(27) Fujita, T.; Ito, Y.; Tan, Y.; Yamaguchi, H.; Hojo, D.; Hirata, A.; Voiry, D.; Chhowalla, M.; Chen, M. Chemically exfoliated ReS_2 nanosheets. *Nanoscale* **2014**, *6*, 12458−12462.
(28) Al-Dulaimi, N.; Lewis, E. A.; Lewis, D. J.; Howell, S. K.; Haigh, S. J.; O'Brien, P. Sequential bottom-up and top-down processing for the synthesis of transition metal dichalcogenide nanosheets: the case of rhenium disulfide (ReS_2). *Chem. Commun.* **2016**, *52*, 7878−7881.
(29) Wu, K.; Chen, B.; Yang, S.; Wang, G.; Kong, W.; Cai, H.; Aoki, T.; Soignard, E.; Marie, X.; Yano, A.; Suslu, A.; Urbaszek, B.; Tongay, S. Domain Architectures and Grain Boundaries in Chemical Vapor Deposited Highly Anisotropic ReS_2 Monolayer Films. *Nano Lett.* **2016**, *16*, 5888−5894.
(30) Zhang, T.; Jiang, B.; Xu, Z.; Mendes, R. G.; Xiao, Y.; Chen, L.; Fang, L.; Gemming, T.; Chen, S.; Rümmeli, M. H.; Fu, L. Twinned growth behaviour of two-dimensional materials. *Nat. Commun.* **2016**, *7*, No. 13911.
(31) Chaturvedi, A.; Slabon, A.; Hu, P.; Feng, S.; Zhang, K.-k.; Prabhakar, R. R.; Kloc, C. Rapid synthesis of transition metal dichalcogenide few-layer thin crystals by the microwave-induced-plasma assisted method. *J. Cryst. Growth* **2016**, *450*, 140−147.
(32) Zhang, X.-O.; Li, Q.-F. Strain-induced magnetism in ReS_2 monolayer with defects. *Chin. Phys. B* **2016**, *25*, No. 117103.
(33) Manchanda, P.; Skomski, R. Defect-induced magnetism in two-dimensional $NbSe_2$. *Superlattices Microstruct.* **2017**, *101*, 349−353.
(34) Datta, D.; Li, J.; Koratkar, N.; Shenoy, V. B. Enhanced lithiation in defective graphene. *Carbon* **2014**, *80*, 305−310.
(35) Sun, X.; Wang, Z.; Fu, Y. Q. Defect-mediated lithium adsorption and diffusion on monolayer molybdenum disulfide. *Sci. Rep.* **2015**, *5*, No. 18712.
(36) Zhou, L.-J.; Hou, Z. F.; Wu, L.-M.; Zhang, Y.-F. First-principles studies of lithium adsorption and diffusion on graphene with grain boundaries. *J. Phys. Chem. C* **2014**, *118*, 28055−28062.
(37) Sun, X.; Wang, Z.; Fu, Y. Q. Adsorption and diffusion of sodium on graphene with grain boundaries. *Carbon* **2017**, *116*, 415−421.
(38) Zhang, R.; Wu, X.; Yang, J. Blockage of ultrafast and directional diffusion of Li atoms on phosphorene with intrinsic defects. *Nanoscale* **2016**, *8*, 4001−4006.
(39) Horzum, S.; Çakır, D.; Suh, J.; Tongay, S.; Huang, Y.-S.; Ho, C.-H.; Wu, J.; Sahin, H.; Peeters, F. M. Formation and stability of point defects in monolayer rhenium disulfide. *Phys. Rev. B* **2014**, *89*, No. 155433.
(40) Perdew, J. P.; Burke, K.; Ernzerhof, M. Generalized Gradient Approximation Made Simple. *Phys. Rev. Lett.* **1996**, *77*, 3865−3868.
(41) Giannozzi, P.; Baroni, S.; Bonini, N.; Calandra, M.; Car, R.; Cavazzoni, C.; Ceresoli, D.; Chiarotti, G. L.; Cococcioni, M.; Dabo, I.; Dal Corso, A.; Fabris, S.; Fratesi, G.; de Gironcoli, S.; Gebauer, R.; Gerstmann, U.; Gougoussis, C.; Kokalj, A.; Lazzeri, M.; Martin-Samos, L.; Marzari, N.; Mauri, F.; Mazzarello, R.; Paolini, S.; Pasquarello, A.; Paulatto, L.; Sbraccia, C.; Scandolo, S.; Sclauzero, G.; Seitsonen, A. P.; Smogunov, A.; Umari, P.; Wentzcovitch, R. M. QUANTUM ESPRESSO: a modular and open-source software project for quantum simulations of materials. *J. Phys.: Condens. Matter* **2009**, *21*, No. 395502.
(42) Monkhorst, H. J.; Pack, J. D. Special points for Brillouin-zone integrations. *Phys. Rev. B* **1976**, *13*, 5188−5192.
(43) Kokalj, A. Computer graphics and graphical user interfaces as tools in simulations of matter at the atomic scale. *Comput. Mater. Sci.* **2003**, *28*, 155−168.
(44) Momma, K.; Izumi, F. VESTA 3 for three-dimensional visualization of crystal, volumetric and morphology data. *J. Appl. Crystallogr.* **2011**, *44*, 1272−1276.
(45) Barone, V.; Casarin, M.; Forrer, D.; Pavone, M.; Sambi, M.; Vittadini, A. Role and effective treatment of dispersive forces in materials: Polyethylene and graphite crystals as test cases. *J. Comput. Chem.* **2009**, *30*, 934−939.
(46) Peng, Q.; Wang, Z.; Sa, B.; Wu, B.; Sun, Z. Blue phosphorene/MS_2 (M = Nb, Ta) heterostructures as promising flexible anodes for lithium-ion batteries. *ACS Appl. Mater. Interfaces* **2016**, *8*, 13449−13457.
(47) Samad, A.; Shin, Y.-H. MoS2@VS_2 nanocomposite as a superior hybrid anode material. *ACS Appl. Mater. Interfaces* **2017**, *9*, 29942−29949.
(48) Er, D.; Li, J.; Naguib, M.; Gogotsi, Y.; Shenoy, V. B. Ti_3C_2 MXene as a high capacity electrode material for metal (Li, Na, K, Ca) ion batteries. *ACS Appl. Mater. Interfaces* **2014**, *6*, 11173−11179.
(49) Henkelman, G.; Uberuaga, B. P.; Jónsson, H. A climbing image nudged elastic band method for finding saddle points and minimum energy paths. *J. Chem. Phys.* **2000**, *113*, 9901−9904.

DOI: 10.1021/acsami.7b13604
ACS Appl. Mater. Interfaces 2018, 10, 5373−5384

(50) Li, F.; Qu, Y.; Zhao, M. Germanium sulfide nanosheet: a universal anode material for alkali metal ion batteries. *J. Mater. Chem. A* **2016**, *4*, 8905−8912.
(51) Xiao, B.; Li, Y.-c.; Yu, X.-f.; Cheng, J.-b. Penta-graphene: A Promising Anode Material as the Li/Na-Ion Battery with Both Extremely High Theoretical Capacity and Fast Charge/Discharge Rate. *ACS Appl. Mater. Interfaces* **2016**, *8*, 35342−35352.
(52) Meng, Q.; Hu, A.; Zhi, C.; Fan, J. Theoretical prediction of MXene-like structured Ti_3C_4 as a high capacity electrode material for Na ion batteries. *Phys. Chem. Chem. Phys.* **2017**, *19*, 29106−29113.
(53) Tang, W.; Sanville, E.; Henkelman, G. A grid-based Bader analysis algorithm without lattice bias. *J. Phys.: Condens. Matter* **2009**, *21*, No. 084204.
(54) Meng, Q.; Hu, A.; Zhi, C.; Fan, J. Theoretical prediction of MXenes-like structure Ti_3C_4 as a high capacity electrode material for Na ion batteries. *Phys. Chem. Chem. Phys.* **2017**, 29106.
(55) Pollak, E.; Geng, B.; Jeon, K.-J.; Lucas, I. T.; Richardson, T. J.; Wang, F.; Kostecki, R. The Interaction of Li^+ with Single-Layer and Few-Layer Graphene. *Nano Lett.* **2010**, *10*, 3386−3388.
(56) Guo, G.-C.; Wei, X.-L.; Wang, D.; Luo, Y.; Liu, L.-M. Pristine and defect-containing phosphorene as promising anode materials for rechargeable Li batteries. *J. Mater. Chem. A* **2015**, *3*, 11246−11252.
(57) Mortazavi, B.; Rahaman, O.; Ahzi, S.; Rabczuk, T. Flat borophene films as anode materials for Mg, Na or Li-ion batteries with ultra high capacities: A first-principles study. *Appl. Mater. Today* **2017**, *8*, 60−67.
(58) Kulish, V. V.; Malyi, O. I.; Persson, C.; Wu, P. Adsorption of metal adatoms on single-layer phosphorene. *Phys. Chem. Chem. Phys.* **2015**, *17*, 992−1000.
(59) Förster, A.; Gemming, S.; Seifert, G.; Tománek, D. Chemical and Electronic Repair Mechanism of Defects in MoS_2 Monolayers. *ACS Nano* **2017**, *11*, 9989−9996.
(60) Yu, Z.; Pan, Y.; Shen, Y.; Wang, Z.; Ong, Z.-Y.; Xu, T.; Xin, R.; Pan, L.; Wang, B.; Sun, L. Towards Intrinsic Charge Transport in Monolayer Molybdenum Disulfide by Defect and Interface Engineering. 2014, arXiv preprint arXiv:1408.6614. arXiv.org e-Printarchive. http://arxiv.org/abs/1408.6614.

DOI: 10.1021/acsami.7b13604
ACS Appl. Mater. Interfaces 2018, 10, 5373−5384